Journal of Power Sources 185 (2008) 922–926

Contents lists available at ScienceDirect

Journal of Power Sources

journal homepage: www.elsevier.com/locate/jpowsour

Short communication

Electrochemical analysis of hydrogen membrane fuel cells

Naoki Ito[a,*], Satoshi Aoyama[a], Takatoshi Masui[a], Shinichi Matsumoto[a], Hiroshige Matsumoto[b,c], Tatsumi Ishihara[b,c]

[a] Toyota Motor Corporation, Higashifuji Technical Center, Susono, Shizuoka 410-1193, Japan
[b] Department of Applied Chemistry, Faculty of Engineering, Kyushu University, Nishi-ku, Fukuoka 819-0395, Japan
[c] Center for Future Chemistry, Kyushu University, Nishi-ku, Fukuoka 819-0395, Japan

ARTICLE INFO

Article history:
Received 30 April 2008
Received in revised form 23 June 2008
Accepted 6 August 2008
Available online 14 August 2008

Keywords:
Fuel cell
Proton conductor
Intermediate temperature
Hydrogen membrane
AC impedance

ABSTRACT

An electrochemical analysis was conducted with respect to a hydrogen membrane fuel cell with $SrZr_{0.8}In_{0.2}O_{3-\delta}$ electrolyte, which is a new type of fuel cell featuring an ultra-thin proton conductor supported on a dense metal anode. Most of the voltage loss derives from the cathode and the electrolyte, and a small amount of anode polarization was observed only in regions with high current density. The cathode polarization was approximately an order of magnitude lower than that of SOFCs. Furthermore, the conductivity of the film electrolyte was almost identical to that of the sinter at 600 °C; however, it was several times as large at 400 °C. A TEM micrograph revealed that the film electrolyte consists mainly of long columnar crystals, and this crystal structure can be related to the conductivity enhancement below 600 °C.

1. Introduction

Fuel cells with high power density operating at intermediate temperatures (400–600 °C) are considered an ideal power source for future vehicles propelled by liquid fuel. High system efficiency can be achieved since waste heat from the fuel cell can be utilized by the fuel reformer, in which endothermic reforming reactions are performed. Solid oxide fuel cells (SOFCs) are excellent fuel cells with high power density at temperatures higher than 800 °C, however, the need for great start-up energy and expensive materials are two major issues which prevent their application in vehicles.

Fuel cells with high power density at intermediate temperatures have not yet been realized since the ionic conductivity of the candidate electrolyte materials is not high enough. As a result, there has been considerable research aiming at achieving high power density by using thin electrolyte supported on either electrode. Huang et al. has reported a power density of 0.4 W cm^{-2} at 400 °C using 0.1 μm of YSZ as electrolyte supported on Si [1]. Furthermore, Ishihara et al. have reported a power density of 1.6 W cm^{-2} at 700 °C and 0.5 W cm^{-2} at 500 °C using 1 μm of LSGM as electrolyte supported on a Ni/YSZ anode [2]. In previous work, we proposed a new conceptual fuel cell named the hydrogen membrane fuel cell (HMFC), which consists of an ultra-thin proton conductor electrolyte supported on a dense hydrogen membrane anode. The power density of the HMFC was as high as 0.9 W cm^{-2} at 400 °C and 1.4 W cm^{-2} at 600 °C using $BaCe_{0.8}Y_{0.2}O_{3-\delta}$ thin film as electrolyte [3].

Although SOFCs with thin film electrolytes have been successful to a certain extent in achieving high power density at intermediate temperatures, in most cases the power density is not as high as that expected from the thickness of the electrolyte. A detailed electrochemical analysis is needed in order to solve this problem, but only a few research efforts have been reported. Although the introduction of a reference electrode is an effective technique for analyzing fuel cells, Adler has reported that this technique is not effective in the case of SOFCs with thin film electrolyte [4]. In this study, we have performed a detailed electrochemical analysis of the HMFC using an AC impedance technique.

2. Experimental

The test cells were prepared as follows. The $SrZr_{0.8}In_{0.2}O_{3-\delta}$ electrolyte was deposited on a Pd film (80 μm in thickness) by pulse laser deposition. The thickness of the electrolyte was confined in the range of 0.7–6.0 μm by controlling the deposition time, and the thickness was confirmed by SEM cross-section imaging. Next, $La_{0.6}Sr_{0.4}CoO_{3-\delta}$ cathode paste was screen-printed on the coated Pd structure and dried with a heat gun. This procedure was repeated three times in order to make a complete cathode layer, which is

* Corresponding author. Tel.: +81 55 997 7985; fax: +81 55 997 7120.
E-mail address: naoki@ito.tec.toyota.co.jp (N. Ito).

0378-7753/$ – see front matter © 2008 Elsevier B.V. All rights reserved.
doi:10.1016/j.jpowsour.2008.08.004

30 μm thick. The size of the Pd film was 15 mm × 15 mm. The electrolyte and the electrode were coated on the Pd film in the shape of a circle 6 mm in diameter for a total of 0.283 cm^2 effective fuel cell area. Finally, the test cells were sealed using a ceramic adhesive (White Seal produced by Taketsuna Corporation) and heated to the operating temperature. During this period, dry air (400 cm^3 min^{-1}) was supplied to both the anode and the cathode sides. After the start-up procedure, the individual cells were operated at 400, 500 and 600 °C in order to obtain the temperature dependence, and at 400 °C during all other measurements. Humidified hydrogen (200 cm^3 min^{-1}, $p(H_2O)$ = 7.3 kPa) was supplied to the anode side, and humidified air (400 cm^3 min^{-1}, $p(H_2O)$ = 7.3 kPa) was supplied to the cathode side during operation. For the $p(H_2)$ and $p(O_2)$ dependence measurements, the hydrogen concentration was varied between 10% and 100%, and the oxygen concentration was varied between 5% and 100% by the addition of nitrogen. Electrochemical measurements were carried out using a Solartron SI 1287 + 1255B system, and the AC impedance measurements were carried out in a frequency range of 0.1 Hz to 1 MHz with and without bias current. Several bias current values were selected for each fuel cell sample in accordance with the performance of the respective test cell.

The conductivity of the $SrZr_{0.8}In_{0.2}O_{3-\delta}$ sinter was measured for the purpose of comparison with the film electrolyte. The $SrZr_{0.8}In_{0.2}O_{3-\delta}$ sinter supplied by TYK Corporation was used for the conductivity measurements and for the PLD target. The conductivity was measured using a DC 4-point method with platinum paste and wire in a humidified H_2 atmosphere and a humidified O_2 atmosphere ($p(H_2O)$ = 1.9 kPa) at temperatures between 400 °C and 900 °C.

3. Results and discussion

The relation between the fuel cell characteristics on one hand and $p(H_2)$ and $p(O_2)$ on the other was measured for the fuel cell with electrolyte thickness of 2 μm at 400 °C for the purpose of analyzing the AC impedance spectra. The effects of the bias current over the AC impedance spectrum are shown in Fig. 1a. Only one semicircle with peak frequency of 250–2000 Hz (high-frequency semicircle) was seen in the AC impedance spectrum measured without bias current. As the bias current increased, another semicircle with peak frequency around 0.6 Hz (low-frequency semicircle) appeared, and the high-frequency semicircle became smaller. Small jagging was observed in the low-frequency region of the AC impedance spectrum without the bias current. However, the authors decided not to treat this part as a low-frequency semicircle since the data quality was not sufficiently high to recognize it as a semicircle. The influences of $p(H_2)$ in the anode gas and $p(O_2)$ in the cathode gas are shown in Fig. 1b and c. It is clear that the high-frequency semicircle is affected only by $p(O_2)$ and the low-frequency semicircle is affected only by $p(H_2)$. From these results, we could identify the high-frequency semicircle with the cathode polarization and the low-frequency semicircle with the anode polarization. Abe et al. have reported similar peak frequency for the cathode polarization semicircle of SOFC [5]. In some AC impedance spectra, the higher frequency semicircle appears to consist of two semicircles, and can include grain boundary resistance. Although neither the anode nor the cathode polarization is ohmic, we refer to the diameter of the semicircle as the anode or the cathode resistance in this paper. The intercept with the real axis, which represents the total internal resistance, is treated as the electrolyte resistance in the subsequent discussion.

The anode and the cathode resistance are shown in Fig. 2 as a typical example of the dependence of the electrolyte on the current

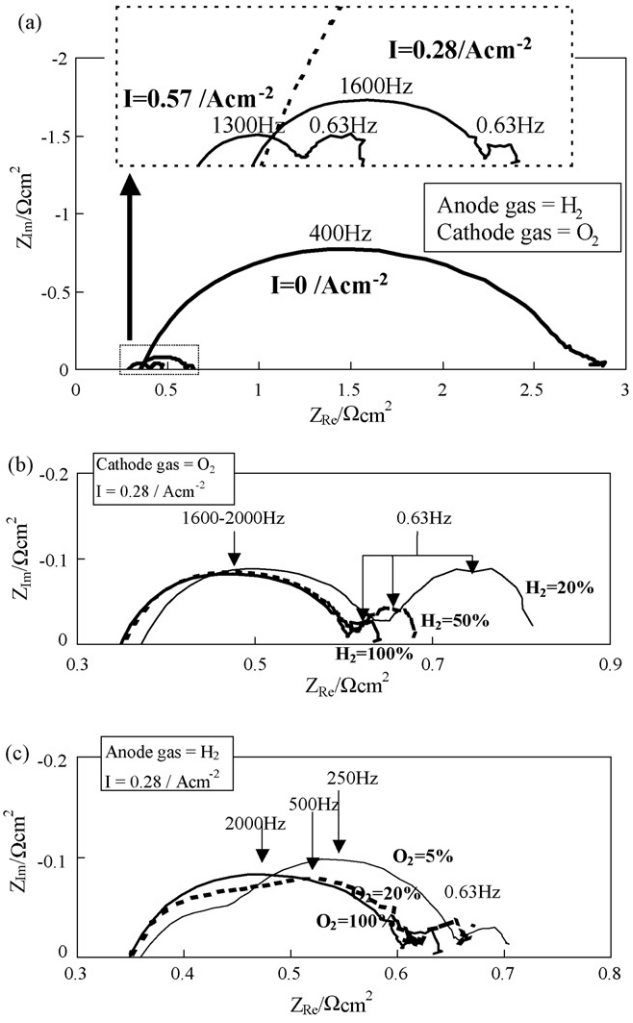

Fig. 1. AC impedance spectra of the test cell with electrolyte thickness of 2 μm at 400 °C. (a) Effects of the bias current, (b) effects of the concentration of H_2 in the anode gas, and (c) effects of the concentration of O_2 in the cathode gas.

density. AC impedance spectra provide only intermittent information about the resistance. Therefore, in order to estimate the polarization or the overpotential, it is necessary to set up a function which fits to the resistance data, followed by integrating it with respect to the current density. We estimated the anode and cathode polarizations, as well as the electrolyte overpotential, as follows.

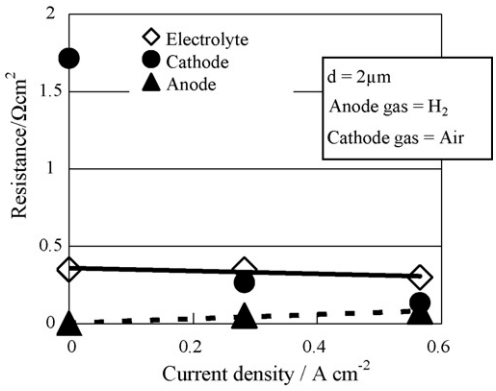

Fig. 2. A typical example of cell resistance as a function of the current density.

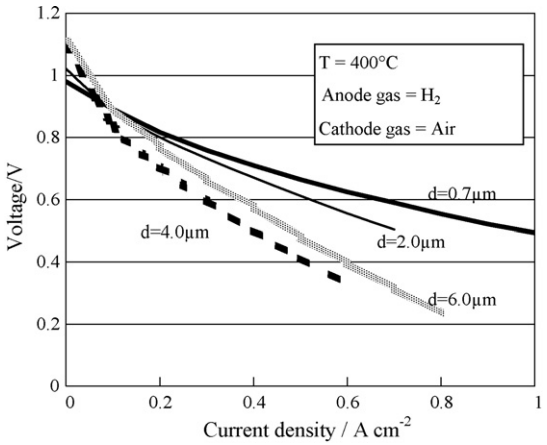

Fig. 3. *V–I* characteristics of test cells with various electrolyte thickness at 400 °C.

At first, we introduced Eqs. (1) and (2) in order to set up the electrolyte resistance and the anode resistance as functions of the current density. These experimental functions are chosen only for the purpose of fitting the experimental data. Although the electrolyte resistance is assumed to be ohmic, we introduced Eq. (2) since the measured electrolyte resistance slightly decreases as the current density increases, which suggests an increase in the local temperature of the test cell. Next, *A*, *B* and *C* were determined such that they fit the function to the experimental data using the least square fitting method. Then, the electrolyte overpotential and the anode polarization were calculated by integrating Eqs. (1) and (2) with respect to the current density. Finally, the cathode polarization was calculated from Eq. (3).

$$\text{electrolyte resistance} = A - B \times I \tag{1}$$

$$\text{anode resistance} = C \times I \tag{2}$$

$$\begin{aligned}\text{cathode polarization} = {} & \text{total polarization} \\ & - \text{electrolyte overpotential} \\ & - \text{anode polarization}\end{aligned} \tag{3}$$

where the total polarization is obtained from the *V–I* characteristics.

The *V–I* characteristics of the test cells for various electrolyte thicknesses are shown in Fig. 3. Higher performance was realized with the test cells with thinner electrolyte, with the exception of two cells whose electrolyte thickness was 4 μm and 6 μm. In this work, we analyzed the AC impedance data with a highly simplified model, after which we made a relatively rough estimate of the overpotential and the polarization. The authors understand the limitations of electrochemical analysis in this work, and intend to conduct more strict and detailed analyses of HMFCs in future work.

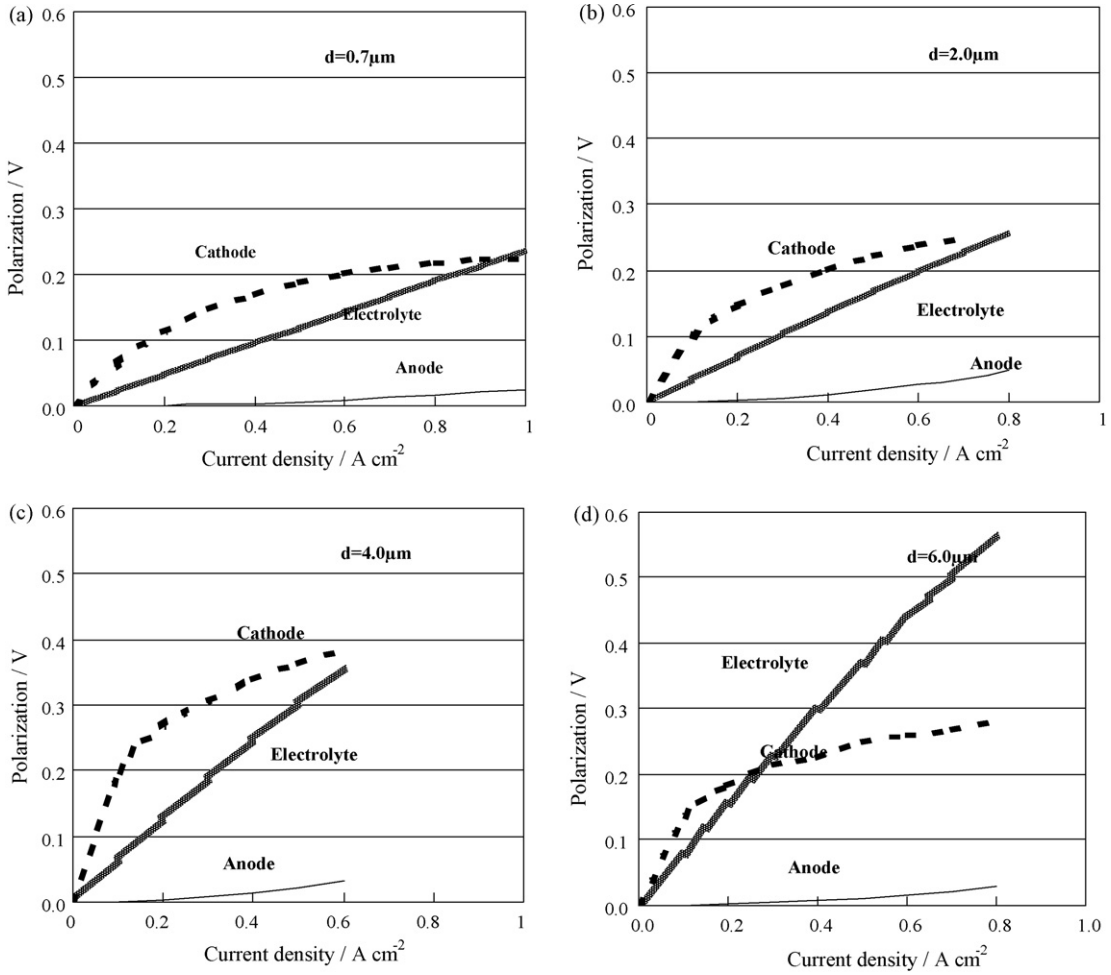

Fig. 4. Electrolyte, anode and cathode polarization as a function of current density at 400 °C in humidified H_2 and air: (a) *d* = 0.7 μm; (b) *d* = 2.0 μm; (c) *d* = 4.0 μm; (d) *d* = 6.0 μm.

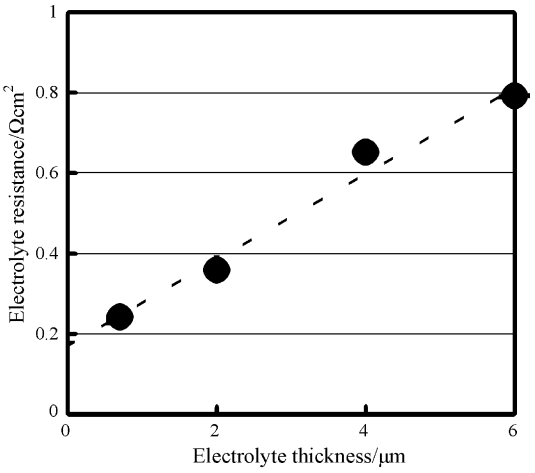

Fig. 5. Electrolyte resistance as a function of electrolyte thickness at 400 °C.

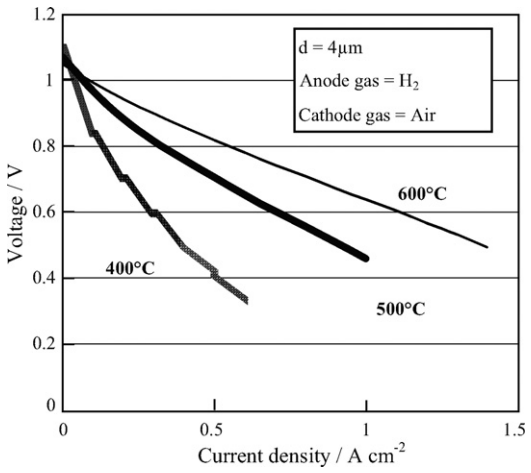

Fig. 6. *V–I* characteristics of the test cell with electrolyte thickness of 4 μm at various temperatures.

The estimated polarization and overpotential are shown in Fig. 4. The major part of the voltage loss was attributable to the electrolyte overpotential and the cathode polarization in all test cells, although there were some deviations in the polarization ratio. In all test cells, the anode polarization was negligible or very small, except in regions with high current density, and it was shown that dense hydrogen membranes work well as anodes in this temperature range. The relationship between the resistance and the thickness of the electrolyte is shown in Fig. 5. The electrolyte resistance was not proportional to its thickness, which explains the existence of an interception on the *Y*-axis. This result suggests that the conductivity of the electrolyte is lower near the anode interface than in other parts of the anode.

Temperature dependence measurements were conducted for the test cell with electrolyte thickness of 4 μm. The *V–I* characteristics for 400 °C, 500 °C and 600 °C are shown in Fig. 6. Higher performance was achieved at higher operating temperatures, and the performance at 600 °C was approximately three times as high as that at 400 °C. The cathode polarization displayed strong temperature dependence, whereby the polarization at 600 °C was approximately 1/4 of that at 400 °C (Fig. 7). The strong temperature dependence and the high peak frequency (250–2000 Hz) suggest that the cathode polarization observed in this study is mainly activation polarization. On the other hand, it was found that the anode polarization depends very weakly on the temperature (Fig. 8), which suggests, together with the low peak frequency around 0.6 Hz, that the anode polarization is mainly concentration polarization. Although a very common cathode material ($La_{0.6}Sr_{0.4}CoO_{3-\delta}$) was used in this study, the measured cathode resistance was approximately an order of magnitude lower than that of SOFCs [7]. Some features of this new concept fuel cell must be related to this large difference, and further study is needed in order to understand it.

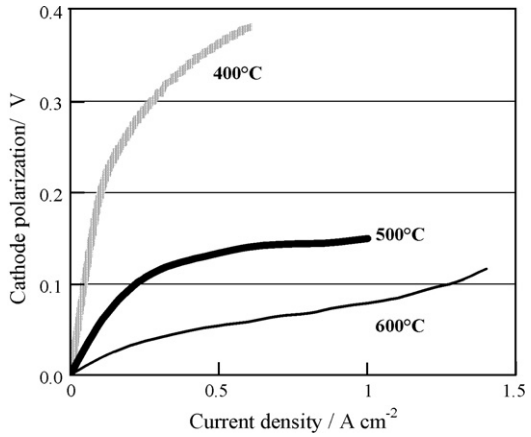

Fig. 7. Cathode polarization as a function of current density.

There were some differences between the theoretical and the measured OCVs, and the comparison is summarized in Table 1. As shown in Table 1, the differences are not affected by the operating temperatures as much as they are affected by the thickness of the electrolyte. This result implies that the difference might be due to physical defects of the film electrolyte.

Arrhenius plots of the conductivity of the bulk and the film are shown in Fig. 9. The film conductivity is calculated from the measured electrolyte resistance at $I = 0$ and the electrolyte thickness. Regarding the bulk conductivity, Yajima has reported the total conductivity of $SrZr_{0.8}In_{0.2}O_{3-\delta}$, and the reported value is similar to our result [6]. The conductivity in a wet O_2 atmosphere is higher than that in a wet H_2 atmosphere at temperatures higher than 600 °C, which implies the appearance of hole conduction. Regard-

Table 1
Open-circuit voltage of singe cells in various conditions

Temperature (°C)	Electrolyte thickness (μm)	Measured OCV (mV)	Theoretical voltage (mV)
400	0.7	980	1142
	2.0	1020	1142
	4.0	1100	1142
	6.0	1110	1142
500	4.0	1070	1123
600	4.0	1048	1102

Anode gas: H_2; cathode gas: air.

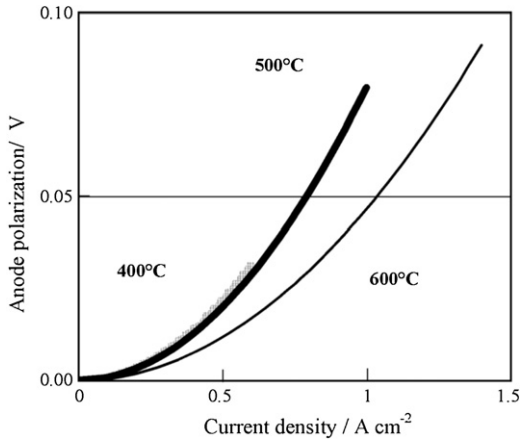

Fig. 8. Anode polarization as a function of current density.

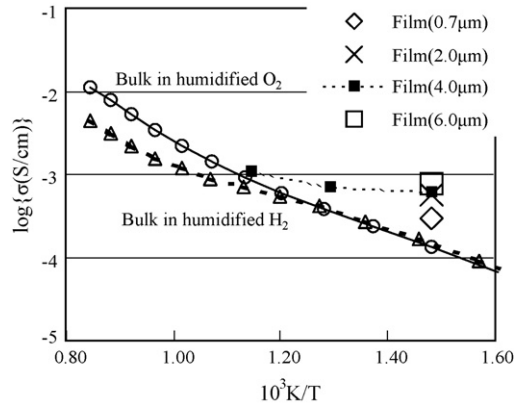

Fig. 9. Temperature dependence of the conductivity of bulk and film $SrZr_{0.8}In_{0.2}O_{3-\delta}$.

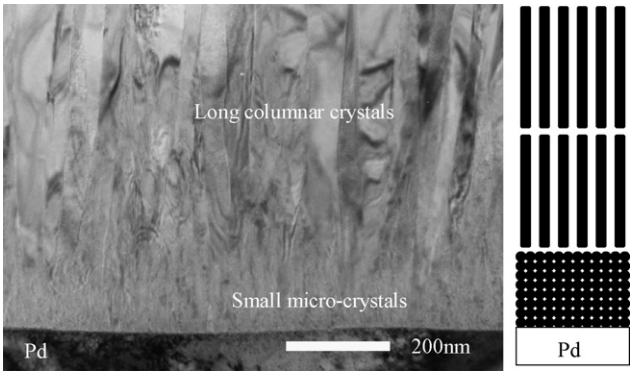

Fig. 10. TEM cross-section image and schematic model of the film electrolyte.

ing the film electrolyte, the effect of hole conduction is assumed to be small according to the measured OCVs of the test cells. The value of the film conductivity was similar to that of the bulk conductivity at 600 °C; however, it was larger at temperatures lower than 600 °C, and several times as large at 400 °C. The film conductivity was also found to be dependent on the electrolyte thickness, whereby higher conductivity was observed for larger values of the electrolyte thickness. A cross-section TEM image of the electrolyte is shown in Fig. 10.

The structure model shown in Fig. 10 can explain the above mentioned characteristics of the film electrolyte. Small micro-crystals are formed near the interface with Pd in the very early stage of the PLD process, followed by the formation of long columnar crystals. The upper part of the film electrolyte has larger grain size than that of a poly-crystal sinter. Therefore, the film electrolyte displays higher conductivity than a sinter at temperatures lower than 600 °C, since the contribution of the grain boundary resistance is large in this temperature range. This model can also explain the non-proportional relation between the thickness and the resistance of the electrolyte shown in Fig. 5. If this model is correct, it would be necessary to improve the cathode polarization and the crystal quality of the film electrolyte around the anode interface in order to realize a higher performance hydrogen membrane fuel.

4. Conclusions

Most of the voltage loss of the HMFC is due to cathode activation polarization and electrolyte overpotential, and small anode concentration polarization was observed only in regions with high current density. The cathode polarization was approximately an order of magnitude lower than that of SOFCs, and displayed strong dependence on the temperature. Although the conductivity of the film electrolyte was almost identical to that of the sinter at 600 °C, it was several times as large at 400 °C. In addition, the conductivity and the thickness of the film electrolyte displayed a non-proportional relation. The TEM micrograph revealed that the film electrolyte consists mainly of long columnar crystals, and this crystal structure can be related to the conductivity enhancement below 600 °C. It is necessary to improve the cathode polarization and the crystal quality of the film electrolyte around the anode interface in order to realize a higher performance HMFC.

References

[1] H. Huang, M. Nakamura, P. Su, R. Fasching, Y. Saito, F.B. Prinz, Journal of the Electrochemical Society 154 (1) (2007) B20.
[2] T. Ishihara, J.W. Yan, H. Matsumoto, ECS Transaction 7 (1) (2007) 435.
[3] N. Ito, M. Iijima, K. Kimura, S. Iguchi, Journal of Power Sources 152 (2005) 200.
[4] S.B. Adler, Journal of the Electrochemical Society 149 (5) (2002) E166.
[5] H. Abe, H. Shimoda, K. Sato, M. Naito, ECS Transactions 7 (1) (2007) 1115.
[6] T. Yajima, H. Suzuki, T. Yogo, H. Iwahara, Solid State Ionics 51 (1992) 101.
[7] J.M. Ralph, C. Rossignol, R. Kumar, Journal of the Electrochemical Society 150 (11) (2003) A1518.